Room-Temperature Soft Magnetic Iron Oxide Nanocrystals: Synthesis, Characterization, and Size-Dependent Magnetic Properties

Yiwei Tan, Zhongbin Zhuang, Qing Peng, and Yadong Li*

Department of Chemistry, Tsinghua University, Beijing 100084, China

Received April 20, 2008. Revised Manuscript Received June 1, 2008

Monodisperse faceted and cubic magnetite nanoparticles were synthesized by the reduction of iron (III) acetylacetonate ($Fe(acac)_3$) with N-methylpyrrole or pyrrole in the presence of the surfactants oleic acid and oleylamine in air. Particle size control can be attained by careful adjustment of the concentrations of the reactants and the surfactants. We also obtained monodisperse maghemite nanoparticles by the oxidation of the as-prepared Fe_3O_4 nanoparticles. The magnetic studies exhibit that increasing the size of iron oxides nanoparticles leads to the enhanced magnetic properties. In particular, the iron oxides nanoparticles with size more than 5 nm are soft ferromagnetic at room temperature.

Introduction

Magnetic iron oxides nanoparticles, including magnetite (Fe_3O_4), maghemite (γ-Fe_2O_3), and wüstite (Fe_xO), are of fundamental scientific and technological importance because of the intrinsic magnetic features combined with the nanosize effects and surface effects. Besides being widely used as ferrofluids,[1] magnetic nanoparticles promise many other applications, such as magnetic resonance imaging contrast agents for molecular imaging,[2–4] AC magnetic field-assisted cancer therapy,[5] and drug targeting.[6,7] The patterned arrays of discrete single domain magnetic nanoparticles are important for applications in high-density information storage.[8,9] Previously, magnetic nanoparticles could be available from aqueous phase synthesis.[4,10–12] In principle, the presence of water is greatly disadvantageous to obtain high-yield discrete iron oxides nanocrystals with sharp size distribution, desired composition, and perfect crystallinity because aqueous phase synthesis can result in the complex aqueous chemistry, such as hydrolysis, hydration, and oxidation. A conceptually different methodology has recently been developed to synthesize iron oxides nanoparticles in organic media,[13–28] which has access to mass production of nearly monodisperse iron oxides nanoparticles at still smaller size scales (several nanometers) that can support only single magnetic domains. Such "bottom-up" approaches involve the high-temperature pyrolysis of iron fatty acid salts (above 300 °C) or the redox reaction of the iron ions at very high temperatures (above 250 °C).

Nevertheless, when the ferromagnetic/ferrimagnetic particle size is reduced below a threshold value, the magnetic anisotropy energy per particle becomes comparable to the ambient thermal energy. The thermal fluctuations cause

* Corresponding author. E-mail: ydli@tsinghua.edu.cn.

(1) Raj, K.; Moskowitz, R. *J. Magn. Magn. Mater.* **1990**, *85*, 233.
(2) Oswald, P.; Clement, O.; Chambon, C.; Schouman-Claeys, E.; Frija, G. *Magn. Reson. Imaging* **1997**, *15*, 1025.
(3) Tromsdorf, U. I.; Bigall, N. C.; Kaul, M. G.; Bruns, O. T.; Nikolic, M. S.; Mollwitz, B.; Sperling, R. A.; Reimer, R.; Hohenberg, H.; Parak, W. J.; Förster, S.; Beisiegel, U.; Adam, G.; Weller, H. *Nano Lett.* **2007**, *7*, 2422.
(4) Hu, F.; Wei, L.; Zhou, Z.; Ran, Y.; Li, Z.; Gao, M. *Adv. Mater.* **2006**, *18*, 2553.
(5) Jordan, A.; Scholz, R.; Wust, P.; Fahling, H.; Felix, R. *J. Magn. Magn. Mater.* **1999**, *201*, 413.
(6) Hergt, R.; Andra, W.; d'Ambly, C. G.; Hilger, I.; Kaiser, W. A.; Richter, U.; Schmidt, H.-G. *IEEE Trans. Magn.* **1998**, *34*, 3745.
(7) Häfeli, U.; Schütt, W.; Teller, J.; Zborowski, M. *Scientific and Clinical Applications of Magnetic Carriers*; Plenum Press: New York, 1997.
(8) Speliotis, D. E. *J. Magn. Magn. Mater.* **1999**, *193*, 29.
(9) Leslie-Pelecky, D. L.; Rieke, R. D. *Chem. Mater.* **1996**, *8*, 1770.
(10) Zhang, Z. J.; Wang, Z. L.; Chakoumakos, B. C.; Yin, J. S. *J. Am. Chem. Soc.* **1998**, *120*, 1800.
(11) Liu, C.; Zou, B.; Rondinone, A. J.; Zhang, Z. J. *J. Am. Chem. Soc.* **2000**, *122*, 6263.
(12) Fried, T.; Shemer, G.; Markovich, G. *Adv. Mater.* **2001**, *13*, 1158.
(13) Sun, S.; Zeng, H. *J. Am. Chem. Soc.* **2002**, *124*, 8204.
(14) Sun, S.; Zeng, H.; Robinson, D. B.; Raoux, S.; Rice, P. M.; Wang, S. X.; Li, G. *J. Am. Chem. Soc.* **2004**, *126*, 273.
(15) Zeng, H.; Li, J.; Wang, Z. L.; Liu, J. P.; Sun, S. *Nano Lett.* **2004**, *4*, 187.
(16) Zheng, R.; Gu, H.; Xu, B.; Fung, K. K.; Zhang, X.; Ringer, S. P. *Adv. Mater.* **2006**, *18*, 2418.
(17) Kovalenko, M. V.; Bodnarchuk, M. I.; Lechner, R. T.; Hesser, G.; Schäffler, F.; Heiss, W. *J. Am. Chem. Soc.* **2007**, *129*, 6352.
(18) Cabot, A.; Puntes, V. F.; Shevchenko, E. V.; Yin, Y.; Balcells, L.; Marcus, M. A.; Hughes, S. M.; Alivisatos, A. P. *J. Am. Chem. Soc.* **2007**, *129*, 10358.
(19) Park, J.; An, K.; Hwang, Y.; Park, J.-G.; Noh, H. J.; Kim, J.-Y.; Park, J.-H.; Hwang, N.-M.; Hyeon, T. *Nat. Mater.* **2004**, *3*, 891.
(20) Jana, N. R.; Chen, Y.; Peng, X. *Chem. Mater.* **2004**, *16*, 3931.
(21) Casula, M. F.; Jun, Y.-W.; Zaziski, D. J.; Chan, E. M.; Corrias, A.; Alivisatos, A. P. *J. Am. Chem. Soc.* **2006**, *128*, 1675.
(22) Peng, S.; Sun, S. *Angew. Chem., Int. Ed.* **2007**, *46*, 4155.
(23) Rockenberger, J.; Scher, E. C.; Alivisatos, A. P. *J. Am. Chem. Soc.* **1999**, *121*, 11595.
(24) Hyeon, T.; Lee, S. S.; Park, J.; Chung, Y.; Na, H. B. *J. Am. Chem. Soc.* **2001**, *123*, 12798.
(25) Cheon, J.; Kang, N.-J.; Lee, S.-M.; Lee, J.-H.; Yoon, J.-H.; Oh, S. J. *J. Am. Chem. Soc.* **2004**, *126*, 1950.
(26) Ahniyaz, A.; Sakamoto, Y.; Bergström, L. *Proc. Natl. Acad. Sci. U.S.A.* **2007**, *104*, 17570.
(27) Redl, F. X.; Black, C. T.; Papaefthymiou, G. C.; Sandstrom, R. L.; Yin, M.; Zeng, H.; Murray, C. B.; O'Brien, S. P. *J. Am. Chem. Soc.* **2004**, *126*, 14583.
(28) Latham, A. H.; Wilson, M. J.; Schiffer, P.; Williams, M. E. *J. Am. Chem. Soc.* **2006**, *128*, 12632.

10.1021/cm801082p CCC: $40.75
Published on Web 07/04/2008

random flipping of the magnetic moment of the nanoparticles with time. As a result, the magnetic moment is not along certain directions any longer such that the nanoparticles become superparamagnetic. Accordingly, the previously prepared iron oxides nanoparticles and even the microsized particles[29,30] are superparamagnetic at room temperature. The permeabilities of superparamagnetic nanoparticles are always greater than 1, but the values are not nearly so great as those of ferromagnets. Such weak magnetic properties restrict the technical and material demands in many aspects on the basis of ferromagnetic features. For example, for high-density information storage, the superparamagnetic relaxation of the magnetization direction in the magnetic data bits with tiny sizes has to be avoided in order to keep the digital data usable.[31] To convert the superparamagnetic nanoparticles to room temperature hard ferromagnet, a complex postsynthesis process, such as annealing or embedding nanoparticles in an antiferromagnetic matrix,[32–34] are required. Therefore, the direct syntheses of high-quality, room-temperature ferromagnetic nanoparticles are highly desirable. Yet, no direct pathways are currently available to obtain room temperature ferromagnetic nanoparticles with low coercivities, i.e., soft magnets.

Herein, we present a novel route toward nearly monodisperse magnetite and maghemite nanoparticles. The syntheses of faceted or cubic Fe_3O_4 nanoparticles were achieved by the reduction of iron(III) acetylacetonate ($Fe(acac)_3$) with N-methylpyrrole or pyrrole in dilute solutions in the presence of the surfactants oleic acid and oleylamine in air. At the same time, the corresponding oxidative polymerizations of these monomers occur. This particular technique allows us to produce Fe_3O_4 nanoparticles at a comparatively low temperature (185 °C). The size of the Fe_3O_4 nanoparticles can be tuned by varying the concentration of the starting reactants. Our protocol does not require a tedious size fractionation procedure to achieve a tight size distribution. The as-prepared magnetic Fe_3O_4 nanoparticles are attracted on a magnetic stirring bar in the reaction vessel such that they can be directly separated from the reaction solution by pouring off the supernatant. In addition, this method can be extended to the synthesis of maghemite nanoparticles by oxidizing the as-prepared magnetite nanoparticles. More dramatically, the magnetic measurements demonstrate that the as-prepared magnetite and maghemite nanoparticles are soft ferromagnets with low coercivities at room temperature and low temperature (10 K) when the particulate size is larger than 5 nm. Furthermore, such soft ferromagnetic properties are dependent on the particle size.

Experimental Section

All chemicals were reagent-grade purity and obtained from commercial sources (Aldrich and Alfa Aesar). All chemicals were used as received. To synthesize 3.2 nm Fe_3O_4 nanoparticles, we loaded 0.4 mmol of $Fe(acac)_3$ into a 100 mL three-neck, round-bottom flask. Under ambient conditions, 5 mL of oleic acid and 4.6 mL of oleylamine were added into the vessel. After the reaction mixture was adequately mixed under magnetic stirring, the vessel was switched to an oil bath. Afterward, 1.2 mmol of N-methylpyrrole dissolved in 0.4 mL of oleylamine was injected into the vessel as soon as the reaction mixture was heated to 185 °C under vigorous stirring. The vigorously stirred reaction solution was kept at 185 °C over a period of 1.5 h, and then promptly cooled to room temperature using cold water to quench the reaction vessel. The ultimate reaction solution was left for 2 days until the as-synthesized magnetite nanoparticles stuck to the magnetic stirring bar. Thus, the black Fe_3O_4 nanoparticles in bulk quantities were obtained by pouring off the supernatant solution. The black product was washed with a large amount of ethanol for 3 times, and subsequently dried. Finally, the Fe_3O_4 nanoparticles can be dissolved in hexane in the presence of a trace amount of oleic acid and oleylamine, giving a dark red-brown colloidal solution. Similarly, 5.4 nm Fe_3O_4 nanoparticles were synthesized with 0.8 mmol of $Fe(acac)_3$ and 2.4 mmol of N-methylpyrrole. 10.3 nm Fe_3O_4 nanocubes were available by utilizing pyrrole as the reductant, the synthetic procedure is the same as that for the synthesis of 3.2 nm Fe_3O_4 nanoparticles except that a mixture consisting of 2 mL of oleic acid, 2 mL of oleylamine, and 6 mL of 1-octadecane was used as the solvent.

The syntheses of γ-Fe_2O_3 nanoparticles were carried out by heating the starting reaction mixture for 9 h but under otherwise conditions identical with those for the production of Fe_3O_4 with N-methylpyrrole and pyrrole as the reductant.

XRD patterns of the Fe_3O_4 nanoparticles were recorded on a Rigaku D/max-2400 diffractometer operated at 40 kV voltage and a 200 mA current with Cu Kα radiation. Magnetic studies were carried out on the nanoparticle powders using a MPMS2 Quantum Design SQUID magnetometer. Prior to magnetic measurements, the as-synthesized iron oxide nanoparticles were washed with ethanol for many times to remove the adsorbed surfactants.

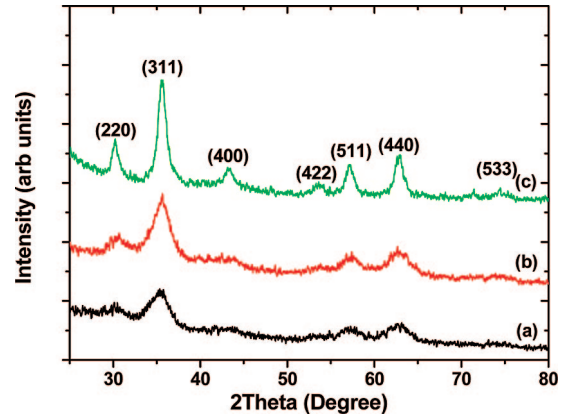

Figure 1. XRD patterns of the Fe_3O_4 nanoparticles synthesized in a solvent consisting of (a, b) 5 mL of oleic acid and 5 mL of oleylamine or (c) 2 mL of oleic acid, 2 mL of oleylamine, and 6 mL of 1-octadecane. Experimental conditions: (a) $[Fe(acac)_3] = 0.04$ M, [N-methylpyrrole] = 0.12 M; (b) $[Fe(acac)_3] = 0.08$ M, [N-methylpyrrole] = 0.24 M; (c) $[Fe(acac)_3] = 0.04$ M, [pyrrole] = 0.12 M.

Results and Discussion

Figure 1 depicts the powder X-ray diffraction (XRD) patterns of the as-prepared Fe_3O_4 nanoparticles with different sizes. The position and relative intensity of all

(29) Deng, H.; Li, X.; Peng, Q.; Wang, X.; Chen, J.; Li, Y. *Angew. Chem., Int. Ed* **2005**, *44*, 2782.
(30) Zhao, L.; Zhang, H.; Xing, Y.; Song, S.; Yu, S.; Shi, W.; Guo, X.; Yang, J.; Lei, Y.; Cao, F. *Chem. Mater.* **2008**, *20*, 198.
(31) Rondinone, A. J.; Samia, A. C. S.; Zhang, Z. J. *J. Phys. Chem. B* **1999**, *103*, 6876.

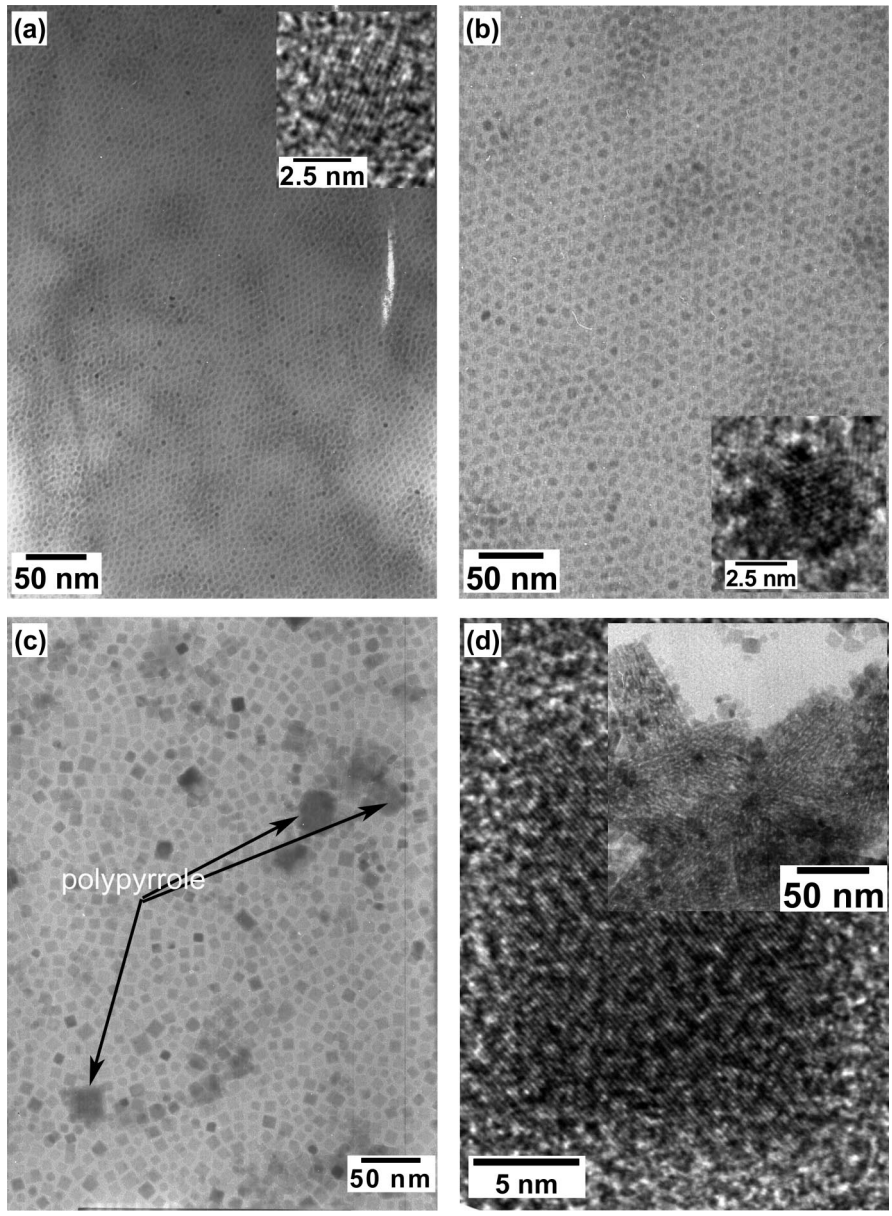

Figure 2. TEM images of (a) 3.5, (b) 5.6, and (c) 10.6 nm Fe_3O_4 nanoparticles synthesized in a solvent consisting of (a, b) 5 mL of oleic acid and 5 mL of oleylamine or (c, d) 2 mL of oleic acid, 2 mL of oleylamine, and 6 mL of 1-octadecane. Experimental conditions: (a) $[Fe(acac)_3] = 0.04$ M, [N-methylpyrrole] = 0.12 M; (b) $[Fe(acac)_3] = 0.08$ M, [N-methylpyrrole] = 0.24 M; (c, d) $[Fe(acac)_3] = 0.04$ M, [pyrrole] = 0.12 M.

Scheme 1. Reaction Equation for the Synthesis of Fe_3O_4 Nanoparticles

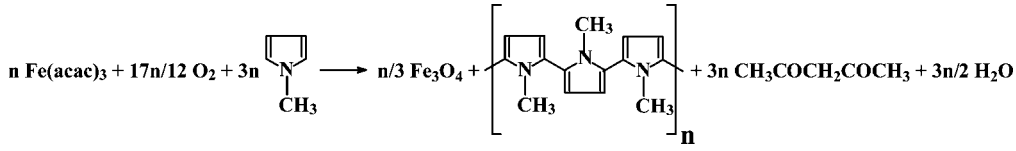

diffraction peaks match well with a cubic spinel structure of magnetite. The mean crystalline sizes of the Fe_3O_4 nanoparticles are calculated to be 3.2, 5.4, and 10.3 nm by measuring the peak widths of the X-ray diffraction lines according to the Debye−Scherrer equation ($D = 0.9\lambda/\beta\cos\theta$). The transmission electron microscopy (TEM) micrographs in Figures 2a and b show that the faceted Fe_3O_4 nanoparticles prepared with N-methylpyrrole as the reductant are monodisperse and self-assemble into order hexagonal closed packing. The mean diameters of the Fe_3O_4 nanoparticles prepared in the presence of 0.04 and 0.08 M $Fe(acac)_3$ are 3.5 and 5.6 nm, respectively, which are in accord with the XRD measurements. Further structural information on the as-synthesized Fe_3O_4 nanoparticles can be obtained from the high resolution TEM (HRTEM) images (the insets in Figures 2a and b). The lattice fringes in the images correspond to a group of lattice planes within a single particle, indicating that the as-synthesized Fe_3O_4 nanoparticles are consistently single crystal. The distances between two adjacent planes are 2.57 (inset in Figure 2a) and 2.92 Å (inset in Figure 2b), corresponding to (311) and (220) planes, respectively.

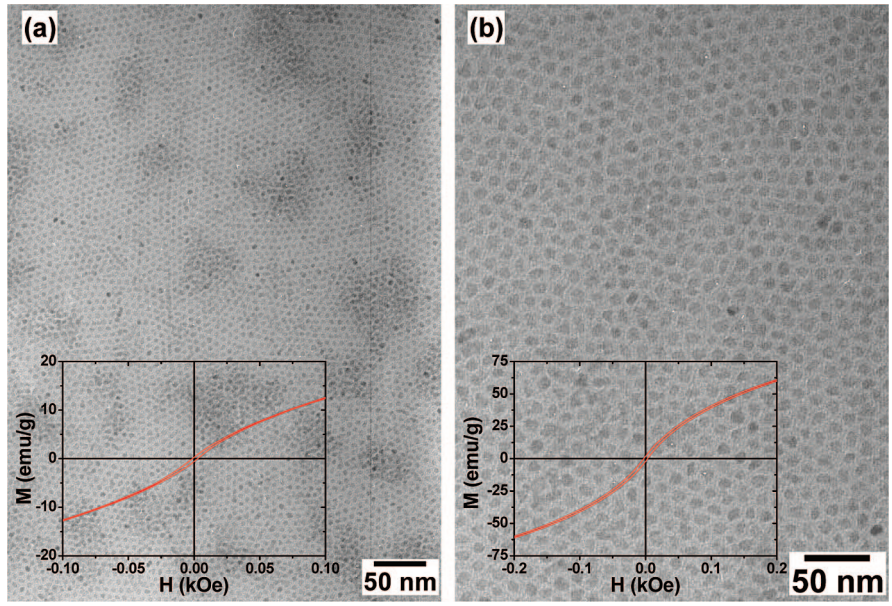

Figure 3. TEM images of the γ-Fe_2O_3 nanoparticles prepared in a solvent consisting of 5 mL of oleic acid and 5 mL of oleylamine. Experimental conditions: (a) [$Fe(acac)_3$] = 0.04 M, [N-methylpyrrole] = 0.12 M; (b) [$Fe(acac)_3$] = 0.08 M, [pyrrole] = 0.24 M. The corresponding room temperature hysteresis loop is shown on the smaller scale in the inset. The coercivity is (a) 6.4 and (b) 11.3 Oe.

When pyrrole is used as the reductant, small regular Fe_3O_4 cubes with an average edge length of 10.6 nm (SD 15%) are yielded. The average domain size determined by the statistical analysis of the TEM micrographs are consistent with that determined by peak widths of the XRD pattern (Figure 1c and the Supporting Information). Additionally, a number of magnetite nanoparticles is stained with polypyrrole in some domains. A similar phenomenon is also observed between the Fe_3O_4 nanoparticles and poly(N-methylpyrrole). HRTEM image shows that these nanoparticles consistently possess the single-crystalline nature, as indicated by the atomic lattice fringes in Figure 2d. The distances between two adjacent lattice planes are 2.07 Å, corresponding to (400) planes in the spinel-structured Fe_3O_4. The structure of the produced polypyrrole is clearly characterized by the TEM observations (inset in Figure 2d). The most impressive aspect of the polyprrole is the ordered lamellar nanostructure with an interlayer distance of 2.7 nm, probably templated by the oleic acid molecules. The similar structures can be found in the poly(N-methylpyrrole).

In our experiments, oxygen is indispensable for the generation of magnetite. The reaction progression is described in Scheme 1. Unlike the high-temperature reaction of $Fe(acac)_3$ in the presence of 1,2-hexadecandiol,[13,14] the redox reaction between $Fe(acac)_3$ and N-methylpyrrole or pyrrole leads to a complete conversion of the Fe(III) to Fe(II) under a flow of an inert gas (nitrogen or argon) at a relatively low temperature (180−185 °C). We thus speculate that the formation of Fe_3O_4 nanoparticles involves the thermal decomposition of acetylacetonate and a subsequent reaction with iron ions in an alternative approach reported by Sun et al.[13,14] In addition, the requirement of reactant oxygen also excludes the possibility of reducing Fe(III) to Fe atoms. The as-synthesized magnetite nanoparticles can be oxidized to maghemite nanoparticles by heating the starting reactants for 9 h at 185 °C in air. The transformations of Fe_3O_4 to γ-Fe_2O_3 can be confirmed by Raman spectroscopy because the Raman spectra of Fe_3O_4 and γ-Fe_2O_3 are markedly different.[19] Comparison of the Raman spectra of the as-synthesized samples with reference samples reveals that a pure phase of Fe_3O_4 and γ-Fe_2O_3 is, respectively, obtained after a different reaction period of 1.5 and 9 h (see the Supporting Information). It is observable from the TEM images in Figure 3 that the γ-Fe_2O_3 nanoparticles synthesized with N-methylpyrrole or pyrrole as the reductant are nearly monodisperse. Compared to the Fe_3O_4 nanoparticles synthesized at the same concentrations of the reactants, the mean diameters of the γ-Fe_2O_3 nanoparticles increase to 4.6 and 7.8 nm, respectively, while the morphologies remain unchanged.

Figure 4 displays the hysteresis loops of the as-synthesized Fe_3O_4 nanoparticles measured at 10 K and room temperature. The insets at the bottom show the room-temperature hysteresis loops on the smaller scale. It can be found that the 3.2 nm magnetite nanoparticles are superparamagnetic. However, the larger magnetite nanoparticles are ferromagnetic despite the small coercivity fields and the small remanent fields, suggesting the increased magnetocrystalline anisotropy. The hysteresis loops exhibit a larger magnetic saturation value as well as a much larger coercive field at 10 K. The magnetic properties are dependent on the size and surface state of the Fe_3O_4 nanoparticles. The bigger magnetic nanoparticles generally have the higher magnetic saturation value. At room temperature, the magnetic saturation values of the 5.4 and 10.3 nm Fe_3O_4 nanoparticles are 45 and 134 emu/

(32) Sun, S.; Murray, C. B.; Weller, D.; Folks, L.; Moser, A. *Science* **2000**, *287*, 1989.
(33) Kang, S.; Miao, G. X.; Shi, S.; Jia, Z.; Nikles, D. E.; Harrell, J. W. *J. Am. Chem. Soc.* **2006**, *128*, 1042.
(34) Skumryev, V.; Stoyanov, S.; Zhang, Y.; Hadjipanayis, G.; Givord, D.; Nogues, J. *Nature* **2003**, *423*, 850.

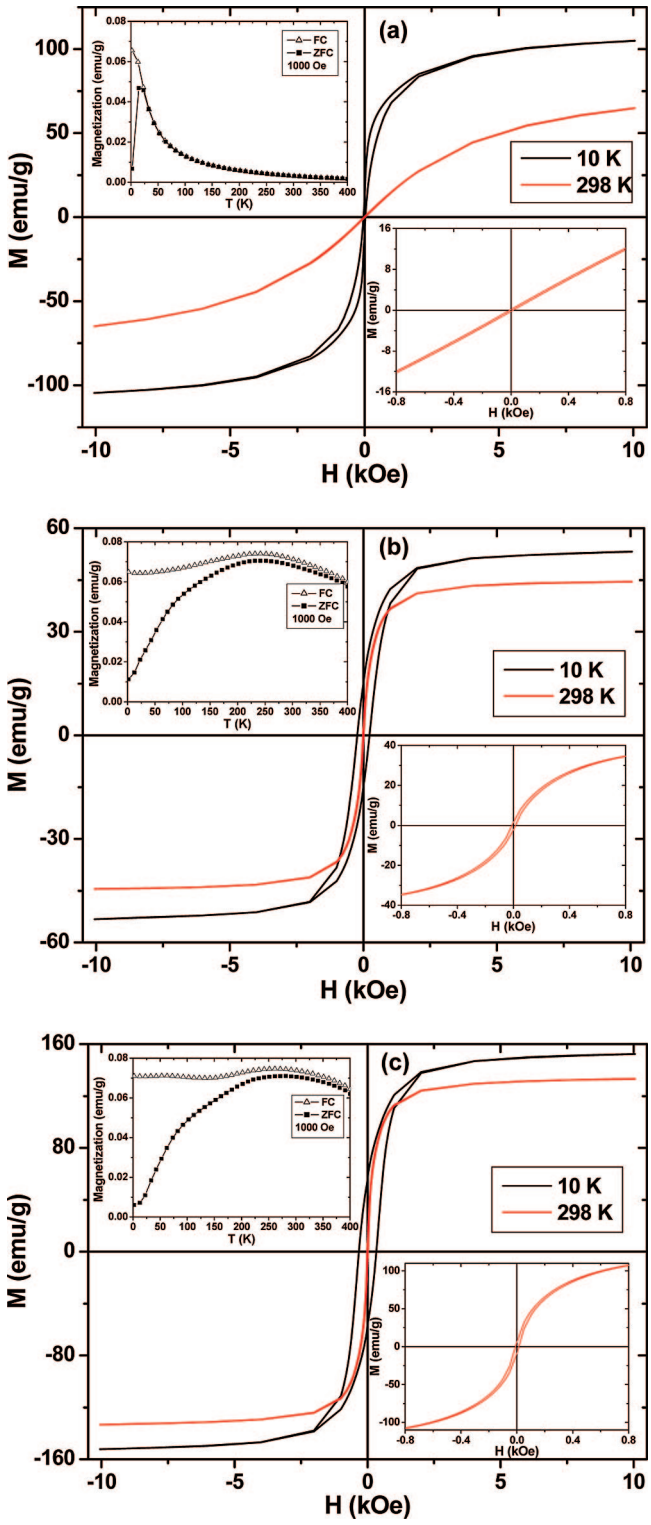

Figure 4. Hysteresis loops of the (a) 3.2, (b) 5.4, and (c) 10.3 nm Fe_3O_4 nanoparticles measured at 10 and 298 K. The insets show the corresponding room temperature hysteresis loops on the smaller scale (bottom) and zero-field-cooled (ZFC) and field-cooled (FC) magnetization in an applied field of 1000 Oe (top).

g, respectively, but the smallest 3.2-nm Fe_3O_4 nanoparticles can not be magnetically saturated in fields up to 1 T. The corresponding value reaches 54, 154, and 106 emu/g at 10 K, respectively. As compared to that of 3.2 nm Fe_3O_4 nanoparticles, the low saturation magnetization of the 5.4 nm Fe_3O_4 nanoparticles may be due to the presence of a magnetic dead or antiferromagnetic layer on the surface.[35–37] The coercivities of the 5.4 and 10.3 nm nanoparticles are 12 and 229, and 15 and 322 Oe at 298 and 10 K, respectively. The low coercivities illustrate that the as-synthesized Fe_3O_4 nanoparticles are soft magnets. For the large magnetic nanoparticles, the effects of thermal agitation, surface spin-canting, and a surface magnetic dead layer become less dominant,[38,39] leading to the enhanced magnetic properties. Apparently, these magnetite nanoparticles are more stable against thermal fluctuations.

Shown in the top insets of Figure 4 is the temperature dependence of the magnetization for field-cooled (FC) and zero-field-cooled (ZFC) Fe_3O_4 nanoparticles under an applied magnetic field of 1000 Oe. The FC and ZFC magnetization curves are split below blocking temperature (T_B, the transformation temperature from ferromagnetism to superparamagnetism) and overlap with each other above T_B as the remanence and coercivity have vanished. For the 3.2 nm Fe_3O_4 nanoparticles, the T_B is about 25 K. Increasing the particle size to 5.4 and 10.3 nm gives rise to an enhancement of T_B up to 330 and 360 K, respectively, which further confirms room temperature ferromagnetism of the larger Fe_3O_4 nanoparticles. Another striking feature is that the FC curves of 5.4 and 10.3 nm Fe_3O_4 nanoparticles show the magnetic moment value increased and then dropped at around 250 K as the temperature decreased. At the same time, the corresponding ZFC curves display two peaks around 100 and 250 K, respectively. The reduced spacing between the magnetite nanocrystals caused by removal of surfactants renders stronger magnetic dipole coupling, resulting in an increase in magnetization toward a broad maximum close to room temperature.[40] In addition, we assume that the formation of the ordered lamellar nanostructures of the conducting polymers may play an important role in increasing the magnetocrystalline anisotropy. This is likely because of the more ordered orientation of Fe^{2+} ions in the crystal lattices that is templated by the ordered lamellar nanostructures. Likewise, such room-temperature soft magnetic behaviors are also observed for the as-synthesized γ-Fe_2O_3 nanoparticles (insets in Figure 3 and the Supporting Information).

Such soft magnetic nanoparticles are readily magnetized and demagnetized. To verify this characteristic, we use a small magnet with a surface field of ~3000 G to attract the Fe_3O_4 nanoparticles in a vial, as shown in Figure 5. Interestingly, all the 5.4 and 10.3 nm Fe_3O_4 nanoparticles in vial A and B can be attracted to the vial walls after 12 h and be redispersed into a colloidally stable dispersion in solution as soon as the small magnet is removed (images b and c in

(35) Pankhurst, Q. A.; Pollard, R. J. *Phys. Rev. Lett.* **1991**, *67*, 248.
(36) Tang, Z.; Sorensen, C. M.; Klabunde, K. J.; Hadjipanayis, G. C. *Phys. Rev. Lett.* **1991**, *67*, 3602.
(37) Chen, J.; Sorensen, C. M.; Klabunde, K. J.; Hadjipanayis, G. C.; Devlin, E.; Kostikas, A. *Phys. Rev. B* **1996**, *54*, 9288.
(38) Morales, M. P.; Veintemillas-Verdaguer, S.; Montero, M. I.; Serna, C. J.; Roig, A.; Casas, L.; Martinez, B.; Sandiumenge, F. *Chem. Mater.* **1999**, *11*, 3058.
(39) Thomson, T.; Toney, M. F.; Raoux, S.; Lee, S. L.; Sun, S.; Murray, C. B.; Terris, B. D. *J. Appl. Phys.* **2004**, *96*, 1197.
(40) Dai, J.; Wang, J.-Q.; Sangregorio, C.; Fang, J.; Carpenter, E.; Tang, J. *J. Appl. Phys.* **2000**, *87*, 7397.

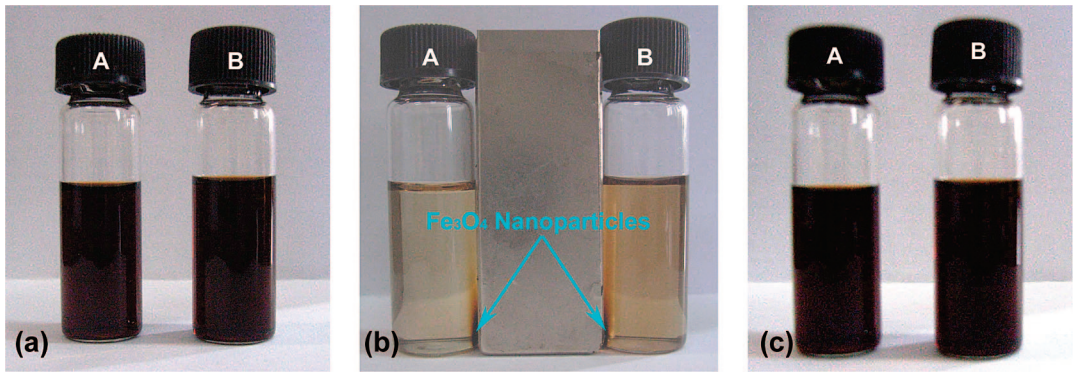

Figure 5. The optical images of the (vial A) 10.3 and (vial B) 5.4 nm Fe_3O_4 nanoparticles dispersed in hexane: (a) before being attracted by a magnet, (b) being attracted by a magnet, and (c) after removing the magnet.

Figure 5). This property is important for efficient bioseparation. For the 3.2 nm Fe_3O_4 nanoparticles, such separation by magnetic attraction is uncompleted even after a longer time of 24 h.

In conclusion, we have established a new platform to use N-methylpyrrole or pyrrole as a reductant for the synthesis of monodisperse magnetite and maghemite nanoparticles with different diameters and shape. These iron oxide nanoparticles exhibit room-temperature soft and enhanced magnetic properties with an increasing the particulate size. Such soft magnetic nanoparticles may serve as microwave devices, magnetic shielding, transformers, and recording heads.

Acknowledgment. We thank Prof. Jinping Chen of The Department of Physics, Peking University, for valuable discussion. This work was supported by National Science Foundation of China (NSFC, 90606006), the State Key Project of Fundamental Research for Nanoscience and Nanotechnology (2006CB932300), and the Key Grant Project of Chinese Ministry of Education (306020).

Supporting Information Available: Detailed characterization of Raman spectra of the iron oxides nanoparticles, more TEM images and size-histogram of the cubic Fe_3O_4 nanoparticles, and the room-temperature hysteresis loops of the γ-Fe_2O_3 nanoparticles on the larger scale. These materials are available free of charge via the Internet at http://pubs.acs.org.

CM801082P